Composites & nanocomposites

A combined theoretical and experimental investigation of the valorization of mechanical and thermal properties of the fly ash-reinforced polypropylene hybrid composites

Atul Kumar Maurya[1], Rupam Gogoi[1], Sushanta K. Sethi[1], and Gaurav Manik[1,*]

[1] *Department of Polymer and Process Engineering, Indian Institute of Technology Roorkee, Saharanpur Campus, Paper Mill Road, Saharanpur, UP 247001, India*

ABSTRACT

Fly ash (FA) particles were surface modified with cetyltrimethylammonium bromide (Ctab) and hybridized with graphene oxide (GO) and carboxymethyl cellulose (CMC) separately to increase interfacial adhesion with the polypropylene (PP) matrix. For a 5 wt.% CMC-hybridized FA, and Ctab-treated FA-filled PP composite, the highest increase in tensile (13% and 7%) and flexural (30% and 25%) strength was observed compared to pristine PP. The functionalization on FA surface was confirmed by ATR-IR analysis. Morphological study using FE-SEM showed that FA particles were successfully carried on to CMC and GO surfaces. An increment in melting temperature by $\sim 3\,°C$ was obtained. Improved thermal stability of the composites was confirmed from TGA analysis. The molecular dynamics (MD) simulations were carried out for all the three modification and it predicted highest interfacial interaction in case of Ctab-FA-reinforced PP composite.

GRAPHICAL ABSTRACT
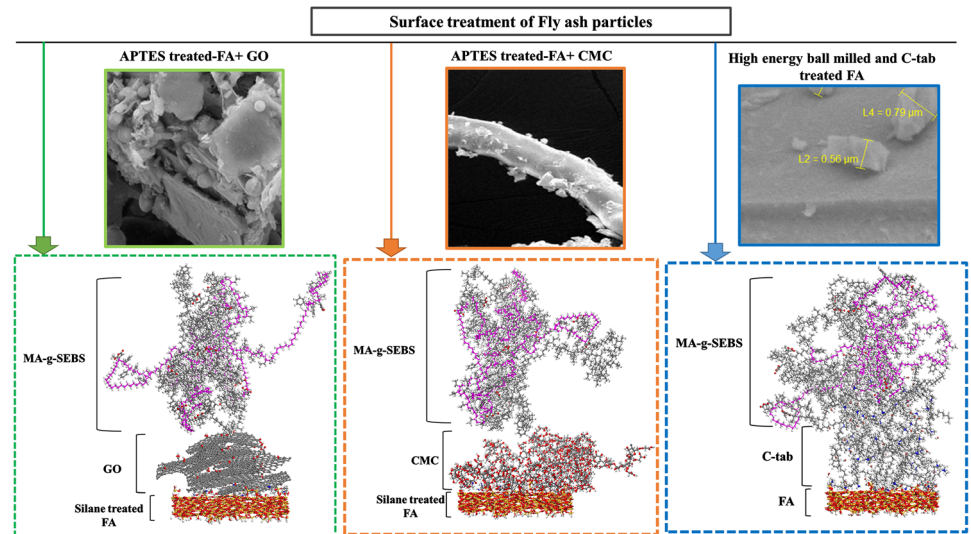
Abbreviations

APTES   (3-Aminopropyl) triethoxysilane
Ctab-FA   Ctab-treated FA reinforcement
GO-FA   GO-hybridized FA reinforcement
CMC-FA   CMC-hybridized FA reinforcement
X_c Crystallinity
SEBS   Styrene ethylene butylene styrene
MA   Maleic anhydride
MA-g-SEBS MA-grafted SEBS

Introduction

Industrial growth is significant for the economic upliftment and urbanization of human civilization, but in parallel to this, it also creates a lot of non-disposable wastes. For instance, due to the high demand for electricity in households and industries, it has been expected that there would be a proportional increase in thermal power generation and also in the generated wastes like FA. In India, as per the report published in Brooking [1], thermal power plants have accomplished more than 80% electricity against the demand between 2009 and 2018. The coal used in these thermal power plants is finally converted to FA and other by-products after combustion. The highest FA content (30–45%) has been reported for Indian coal compared to coals imported from foreign countries [2, 3]. As per the report in India, a total of 217.04 millions ton of FA was generated in 2018–2019 [2, 3]. FA waste has, however, key worrying concerns associated with human health and the surroundings. The existence of alumina, silica and other metals in FA pollutes the soil and groundwater [4, 5] and becomes the reason for many diseases related to the lungs [6]. Even health-hazardous elements like Cd, Cr, Ni, Pb, and V have been reported to be present in FA in low concentrations [7, 8]. Researchers from various fields used numerous acidic wastes to counter the alkalinity and inhibit heavy metals in FA [9–11]. For instance, vinegar residue vermicompost, fruit peel, sewage sludge, and organic agricultural wastes can be used for the same [9–11].

Furthermore, as per a report internationally, 25% of total FA production is used in zeolite synthesis [12], construction industries [13], and ceramic sectors [14–16]. China is the only country utilizing 70% of its FA generated [17]. Therefore, in addition to the

aforementioned applications, extensive use of FA in polymer composites as a reinforcement can be a benign effort in helping the environment and motivating proper waste management. It is worth mentioning here the basic difference between fillers and reinforcement is whether the primary function of material is enhancing the property profiles of the base matrix (BM). If there is a significant increment in some specific properties of the BM /resin, then that inclusion must be treated as reinforcement.

Untreated and non-ball milled FA has a very smooth surface with a spherical shape, which did not provide excellent wettability and dispersion inside the polymer matrix. Furthermore, zero interaction between polymer matrix and agglomeration of FA leads to poor mechanical properties of the formulated polymer composites. Also, limitations of small specific surface area, organically inert, and complex structure of FAs have pushed the researchers to treat or hybridize FA to achieve its chemical activation. [17]. Nonetheless, surface-treated FA offers the benefits of being low cost, good reinforcement, and good processability. Furthermore, to make FA a useful reinforcement and increase its interaction with polymer matrix, prior coating with a coupling agent has been reported by several researchers [17].

Expanding the research, Sengupta et al. have utilized palmitic acid [18] and furfuryl palmitate [19] treated FA and reported enhanced impact properties of the composites in comparison with PP. Sridhar et al. [20] fabricated composites from FA and waste tire powder and revealed that the former possessed better affinity and adhesion toward the rubbery phase in comparison with the plastic phase. Composite foams made from FA and polyurethane have been studied by Kuznia [21]. This composite foam offered better thermal and mechanical properties in comparison with unmodified polyurethane foam. Goh et al. [22] fabricated epoxy composite by reinforcing FA from post-municipal solid waste incineration. Only a limited number of composites have been reported showing mechanical properties better than the reinforced polymer matrix. However, FA treated with colloidal mesoporous silica earlier has shown improvement in mechanical properties [22]. Yang et al. [23, 24] reported in situ grafting through neutralization reaction between surfaces of the carboxylic group of alkene molecules of the carboxylated polymer matrix and metal oxides of the FA particles and achieved higher tensile strength than

the BM. However, this methodology is not fully green and sustainable and can cause serious environmental and health issues during the processing of the reagents.

To overcome the limitations of insignificant increase in tensile strength reported in our previous study, this research employs coupling agent coated or hybridized FA particles to formulate FA reinforced PP composites with enhanced tensile strength, tensile toughness and flexural strength. An increment in the toughness was presumed to be exhibited from the selected BM. A very few studies on the treatment of FA with suitable coupling agents to form useful hybridized FA-reinforced composites have been reported so far. It was presumed that hybridization of FA with carboxymethyl cellulose (CMC) and graphene oxide (GO) has the potential to interact with the polymer matrix and provide better interfacial adhesion and so good mechanical properties [25].

Additionally, it was expected that agglomeration of FA will decrease due to the presence of Ctab and same was reported earlier for FA [26] and microcrystalline cellulose [27]. Hence, silane and mechanochemically Ctab-activated FA under planetary ball milling may give good mechanical properties. Current study employed a polymer blend consisting of PP, SEBS, and MA-g-SEBS having better impact resistance [26, 28] and was used as a BM for the hybrid composites. The selected BM reason for increased tensile toughness of composites, with appropriate impact strength [26, 28], was then used to formulate different treated and hybridized FA-based composites. Evaluation of different mechanical properties, bond energy from molecular simulations, morphology from FE-SEM, thermal behavior from differential scanning calorimetry (DSC) and thermogravimetric analysis were carried out to understand these special composites and are stated as part of this research.
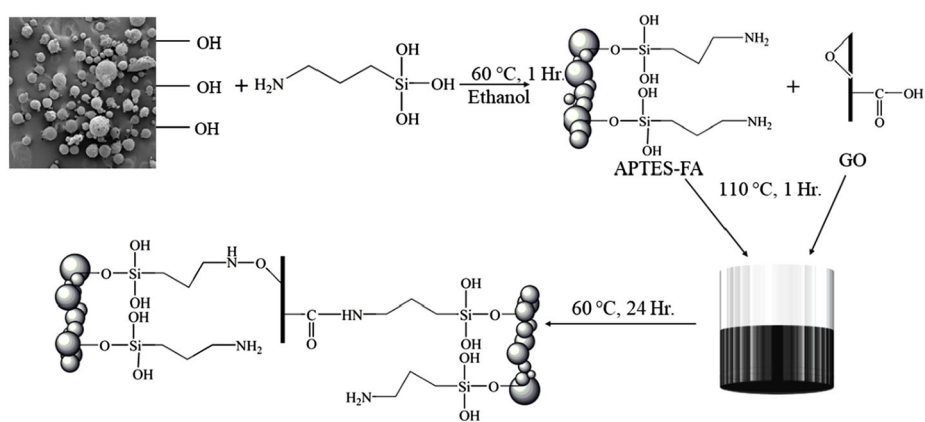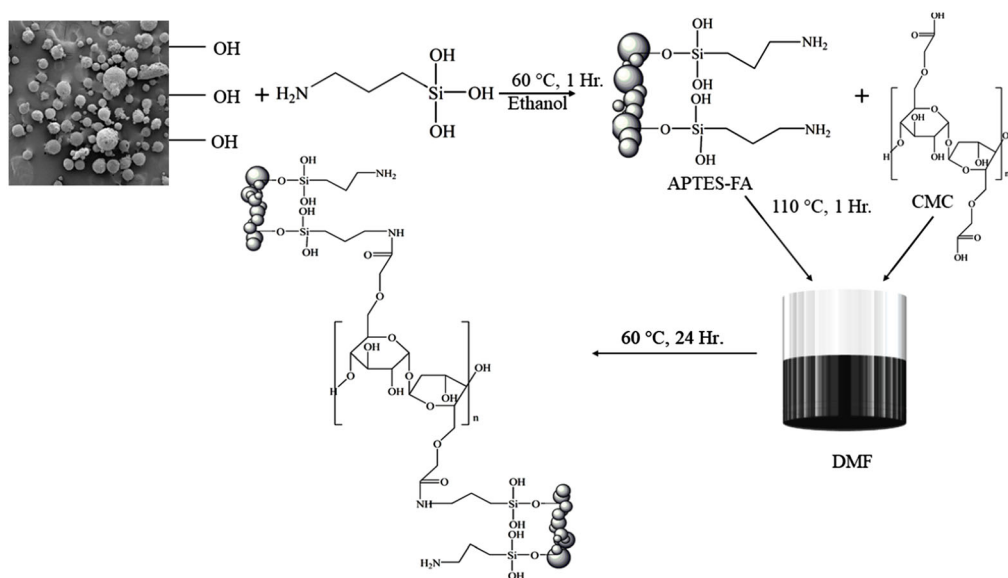
Materials and methods

Materials

Repol H110MA PP with a density of 0.908 g/cm^3 and MFI of 11 g/10 min (230 °C, 2.16 kg) was purchased from Reliance Polymers. SEBS Kraton G1651 H with a specific gravity 0.91 g/cm^3, and styrene/rubber ratio 33–67. MA-g-SEBS under the product name DzBh
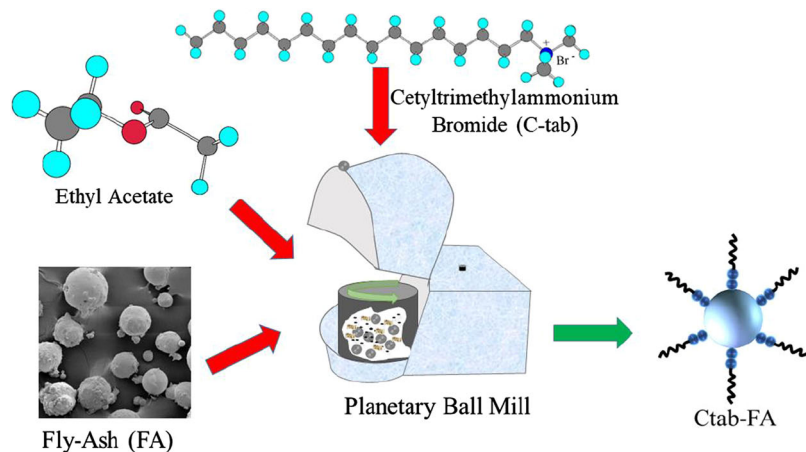
(a)

(b)

(c)

◀ **Figure 1 a** Treatment of FA with Ctab. **b** Hybridization of FA particles with GO. **c** Hybridization of FA with CMC.

Beiwa® 901, having a density 0.96 gm/cm³, MFI of 43 g/ 10 min measured at 200 °C/5 kg and styrene 30%, supplied from China. Cetyltrymethylammonium bromide (Ctab) having melting temperature of 249–253 °C and pH value between 5–7 was supplied by SRL Pvt. Ltd., India. CMC from HIMEDIA under the product name GRM329-500G with viscosity value of 1500–300 cp. GO was purchased from SHILPENT brand with purity up to 99%.

Preparation of elastomeric polymer blends

Based on the mechanical properties such as the tensile, flexural, and notched impact strength of the blends (reported earlier) [28] [26], an optimized mixture of elastomer, coupling agent, and PP was preferred as the BM for composites fabrication. As already reported in our previous study, it was expected that the blend would increase notched impact strength along with interfacial adhesion between reinforcing treated/hybridized FA and BM [26, 28]. A combination of PP (85 wt.%), SEBS (10 wt.%) and MA-g-SEBS (5 wt.%) were optimized and selected as the BM, similar to those used in the previous work [26, 28]. Rheomix QC Lab compounder was used for mixing the polymer, elastomer, and coupling agent for an appropriate time to achieve a uniform blend of the various phases of BM.

Fly ash

FA (Fillit™ 500 s) holding a density of 0.80–0.53 g/cm³, particle size of 5–500 μm and having a moisture content less than 0.5% was ordered from Petra, India Pvt. Limited. FA was grounded down to a particle size up to ∼ 2 μm on a ball mill supplied by Retsch, India. Grinding speed and time were fixed at 25 Hz for 15 min. Zetasizer, USA was used for measuring most probable size of the FA by using the dynamic light scattering principle.

Silane treatment

FA particles with reduced size (∼ 2 μm) were silane treated from 1 wt.% of APTES dissolved in 90:10 (w/w) ethyl alcohol and water solution at ambient temperature for 1 h. Silane-treated FA has been filtered and kept in a hot oven for drying purposes. After drying for more than 12 h. At 100 °C, received chunks of the oven-dried FA were ball-milled again to break the lumps.

Ctab treatment

In Fig. 1a, a high-energy planetary ball mill supplied from Retsch Germany was used for the mechanochemically activation of FA using ethylene acetate as a medium in a tungsten carbide cylinder. A 10:1 of tungsten carbide balls having a diameter of 10 mm were placed in the cylinder at 250 rpm for 8 h. For every 2 h of milling, a break time of 60 s was given after every 30 min of milling to bypass heat generated during the entire process. After ball milling, FA particles recorded the most probable size of ∼ 900 nm established by DLS (Figure S1) and FE-SEM (Fig. 1g, h).

Graphene oxide (GO) hybridization

The solution blending method was used for the formation of GO-FA hybrid. The formation process of the GO-FA hybrid has been illustrated in Fig. 1b. 1 g of the APTES-treated FA and 1 g of the GO were added to 30 ml of DMF solvent. Ultrasonication was used to disperse both the materials in DMF for 30 min at 40 °C. The mixture containing silane-treated FA and GO in DMF was continuously stirred for 1 h in a water bath kettle at 95 °C with a stirrer speed of 150 rpm. After this, the mixture was filtered and washed with anhydrous ethanol and dried at 60 °C for 24 h in a vacuum oven.

Carboxymethyl cellulose hybridization

Acidification of CMC-Na commercial-grade (Himedia GRM329, viscosity 1500–3000 cp) salt was used for carboxymethyl cellulose (HCMC) synthesis. 1 g of CMC-Na has been added to 100 ml of ethyl alcohol (EtOH) and 10 ml of hydrochloric acid (HCl) (10:1) mixture and stirred for 6 h [29]. The dispersed mixture of CMC and EtOH/HCl has been poured into the distilled water for recovery and followed by washing with acetone. The filtered mixture (HCMC) has been dried at 60 °C for 24 h in a vacuum oven.

Thermal amidation of the HCMC (1 g) has been achieved by the solution blending method for the

formation of CMC-FA hybrid. The formation process of the CMC-FA hybrid has been illustrated in Fig. 1c. One gram of the APTES-treated FA, and 1 g of the CMC was added to the 30 ml of DMF solvent. Ultrasonication was used to disperse both the materials in DMF for 30 min at 40 °C. The mixture containing silane-treated FA and CMC in DMF has been continuously stirred for 1 h in an oil bath kettle at 160 °C with a stirrer speed at 150 rpm. After 4 h, this mixture has been filtered and washed with anhydrous ethanol and dried at 60 °C for 24 h in a vacuum oven.

Sample preparation

Prior to samples fabrication of BM and composites, all the components of the base matrix (PP, SEBS, MA-g-SEBS) and treated/hybridized FA were demoisturized in an air oven (80 °C, 12 h.) followed by a vacuum oven (60 °C, 3 h.). Thereafter, a blend of PP, SEBS, and MA-g-SEBS with respective wt.% of 85, 10, and 5 was selected as the BM, which we already optimized and used successfully in our previous work [26, 28]. Different composites were then formulated, keeping 5 wt.% of FA content fixed in each sample of the composite. [30]. PP, SEBS and coupling agent MA-g-SEBS were fed into the hopper of HAAKE™ Rheomix miniCTW twin screw mixer (Make; ThermoFisher SCIENTIFIC) for polymer blend preparation. The machine's temperature and screw speed were maintained between 185–190 °C at 10–50 rpm.

To avoid any possible agglomeration of the treated and hybridized FA, it was added slowly and separately to the melt blend of the BM. The composite mixture obtained was compounded again in a HAAKE™ MiniCTW (Make; ThermoFisher SCIENTIFIC). The temperature and screw speed were maintained between 185–190 °C at 50 rpm. This melt was transferred to the chamber of the HAAKE™ Minijet II for pushing the melt mix to the mold of the samples uphold a temperature of 60 °C [31, 32].

Testing and characterization

ATR-IR

IR characterization was performed in ATR-IR mode within a range of 4000 cm^{-1} to 500 cm^{-1} on a Perkin Elmer Spectrum 2 Instrument for confirming functional group interactions of the treated and hybridized FA following ASTM D5576-00.

Morphological analysis

Morphological study of the various reinforcements and composites was recorded using the Mira3 Tescan FE-SEM instrument at 5 kV. All the specimens were screwed up on an aluminum stub for gold coating before the test.

Mechanical properties

Tensile and flexural properties

Tensile and flexural properties of the PP, BM and composites were studied on UTM (INSTRON 5kN Model 3365) following the ISO 527 (Specimen type 1BA, Figure S2) and ISO 178 (Samples having a dimension of $80 \times 10 \times 4$ mm^3 by keeping 16×4 mm as the span length, Figure S3) standards, with a crosshead speed of 15 mm/min and 2 mm/min, respectively. At least five samples were tested, and average data for the same were reported. Toughness and elongation at break of the samples have been calculated from the stress *versus* strain curve of the tensile test generated from the UTM.

Hardness testing

Hardness testing of all the samples was carried out using ASTM D2240 standard on a shore D hardness tester (Make: YUZUKI Shore D Hardness). Samples having $80 \times 10 \times 4$ mm^3 dimension were used for recording the shore D hardness.

Thermal properties

Differential scanning calorimetry (DSC)

The DSC was performed using the TA instrument (Discovery series DSC 25) setup as per ASTM D3418-15. 2 heating (from room temperature to 250 °C and -60 °C to 250 °C) and 1 cooling cycle has been provided to a 5 mg samples of each category in an aluminum crucible at 10 °C /min in an inert atmosphere. The following equation was used for determining the percentage crystallinity of all the specimen:
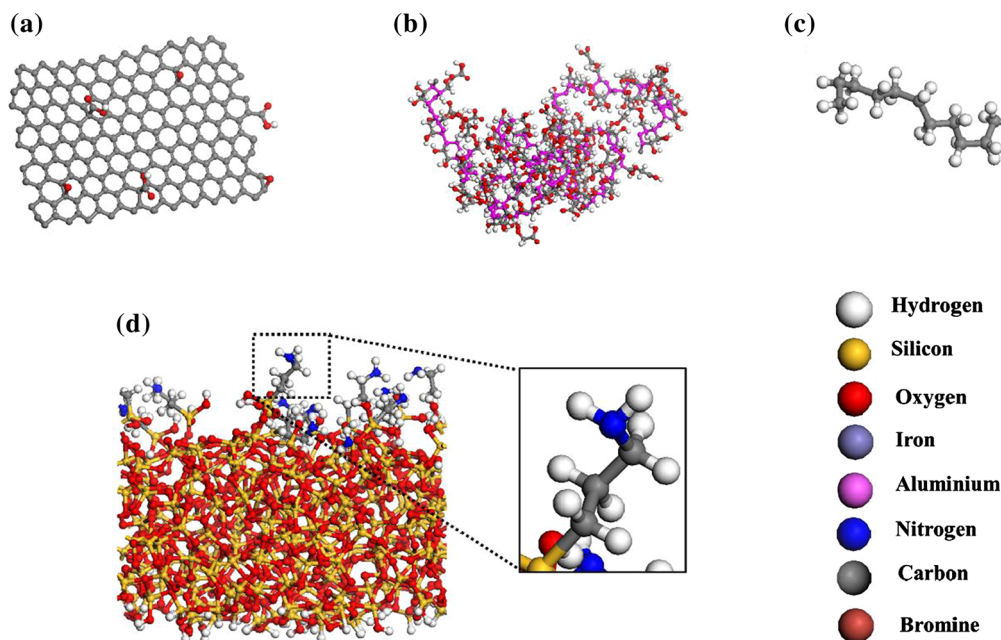
Figure 2 Illustration of the initial configuration of (a) GO, (b) CMC, (c) Ctab, and (d) silane-treated FA. The zoomed-in image displays the terminated silane from the FA surface.

$$\%X_c = \frac{\Delta H}{\Delta H_*} \times 100 \qquad (1)$$

Melting enthalpies of all the samples have been represented by ΔH, while a value of 209 J/g has been selected for ΔH^* which is the melting enthalpy of 100% crystalline PP [33].

Thermal Degradation (TGA)

ASTM E1131 standard was followed for studying the degradation performance of PP, BM, and all the composites. Samples were heated at 10 °C/min from ambient temperature to 800 °C in an inert atmosphere (N_2).

Computational details for the estimation of interaction energy

The interaction among the different surface-treated FA and MA-g-SEBS was theoretically calculated using commercially purchased BIOVIA® Materials Studio™ software [34]. Universal forcefield employing 6–9 Lennard–Jones (LJ) potentials was considered in this work [35, 36]. Cut-off distance of 12.5 Å was used for the van der Waals (vdW) and electrostatic non-bonded interactions. Atom-based and Ewald summation methods were used for calculating vdW

and electrostatic interactions, respectively. Velocity-Verlet algorithm with a time step of 1 fs was used to integrate the equations of motion [37]. Nose–Hoover thermostat was employed for temperature consistency. Periodic boundary conditions (PBC) were employed to all the simulation cells. A similar methodology adopted by Sethi et al. [38] has been employed here to obtain equilibrated simulation cells: (i) Construction of molecular structure/system, (ii) Equilibration of system, and (iii) Post-equilibration/production MD run to estimate the interaction energy. GO was modeled as a sheet of graphene having pendant oxygen containing groups such as carboxylic acid, as seen in Fig. 2a. Atomistic structure of CMC and Ctab is shown in Fig. 2b and c, respectively. Since FA consists majorly of SiO_2 (> 55%), hence, here we considered a slab of hydroxylated crystalline silica as the representation of FA for simplicity. The same was grafted with silanol to represent a silane-treated FA as shown in Fig. 2d. The following Scheme 1 was considered for the grafting of silanol.

Initially density of amorphous cell constructed was kept at 0.4–0.5 g/cm³, which helps to provide sufficient free volume inside the simulation cell and thereby provides an adequate movement to atoms/molecules. Next, geometry optimization was carried out for 5000 steps using the Steepest-decent

Scheme 1 The possible reaction among the silanol and FA surface. Both the possibilities have been incorporated while forming the grafted structure, and shown in Fig. 2d.
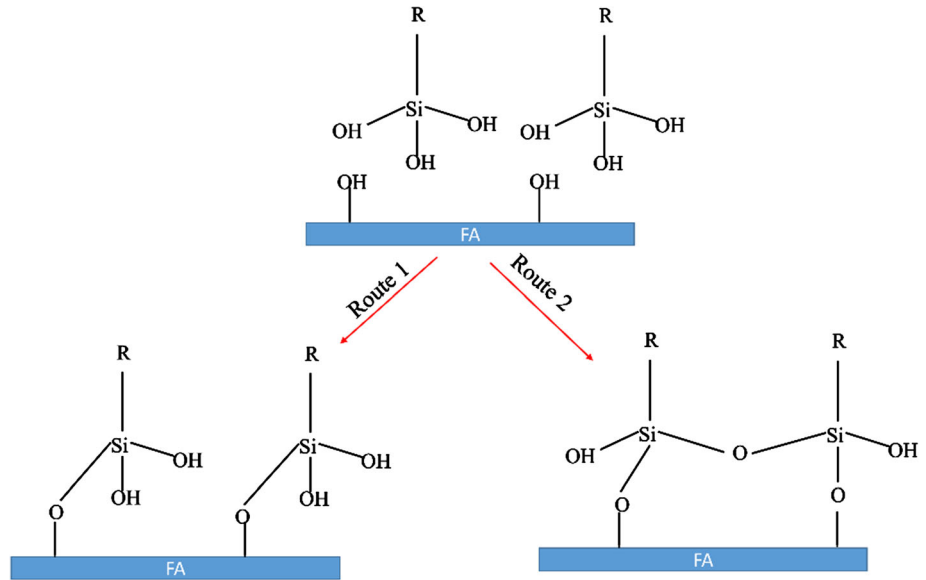
algorithm in ultra-fine quality. Next, the initially constructed molecules were relaxed, equilibrated and randomized by running NVT dynamics run for 300 ps at 750 K. The structure was then subjected to NVT dynamics run for 300 ps at room temperature (298 K). Finally, the initially provided undesired free volume was removed to represent an equilibrated system similar to real-time condition by carrying out NPT dynamics for 300 ps at 298 K under 1 atm. A two-layered system was created from the obtained equilibrated systems for estimating interaction energy, similar procedures were adopted earlier by Sethi et al. [39, 40]. A post-equilibration, i.e., NVT ensemble production run was executed for a time period of 300 ps, and frames were generated after every 5000 steps, which provided a total of 60 frames. These frames were then considered to predict the interaction energy of MA-g-SEBS with GO-FA, CMC-FA and Ctab-FA. The obtained estimates were discussed in the result and discussion section.

The interaction energy was calculated using the following Eq. (2).

$$E_{IE} = E_{AB} - (E_A + E_B) \tag{2}$$

Here, E_{IE} represents the interaction energy, E_{AB} is the total potential energy of the composite or the total system considered. E_A and E_B are the individual potential energy of the components comprising the composite, which in the present case are a single polymer chain of MA-g-SEBS *(A)* and different surface-treated FA *(B)*. The potential energy, E of a system, is estimated as the summation of total bond energy, non-bond energy and energy due to cross-terms as shown in Eq. (3). The total bond energy, $E_{Total\ bond}$ comprises of bond stretching energy (E_b), angle bending energy (E_θ), and dihedral torsion energy (E_ϕ). The non-bonded energy ($E_{Non-bond}$) is composed of vdW energy (E_{vdW}), and electrostatic energy ($E_{Electrostatic}$). The energy due to cross-terms, E_{Cross} arises from the effect of one bonded atom length and angle on another, such as bond–angle and bond–bond cross-terms.

$$\begin{aligned} E &= E_{\text{Total bond}} + E_{\text{Non-bond}} + E_{\text{Cross}} \\ &= (E_b + E + E) + (E_{vdW} + E_{\text{Electrostatic}}) + (E_{\text{Cross}}) \end{aligned} \tag{3}$$

Matrix selection

It was already established in earlier studies that the lowest impact strength was possessed by PP (0.63 kJ/m^2) among impact-modified PP and all the FA and FA-SSL-reinforced hybrid composites [26, 28]. Likewise, toughness which measures the energy absorption before failure showed a value of 13.14 MJ/m^3 for PP (Table 3). BM which is comprising of PP, SEBS and MA-g-SEBS recorded a value of 14.41 MJ/m^3, which is better than PP. Hence, conclusively, we can presume increase in impact properties also improved the tensile toughness of the BM. Also, elongation at break recorded by PP (60.00%) is lesser than BM (80.26%). The improvement in

elongation at break of BM was exhibited due to the decrease in the crystallinity and increase in the molecular chain deformation of the PP [41]. SEBS and MA-g-SEBS develop a more structured network in the matrix and hence restrict the crack propagation during the external force application. Moreover, induced polarity in the ethylene–butylene (EB) block due to the presence MA group in MA-g-SEBS exhibited an impressive toughening effect reported earlier for a MA-g-SEBS/PP blend [42]. Hence, as a result, for better tensile toughness/impact strength and better interfacial adhesion at reinforcement/matrix surface, BM has been chosen as a matrix for composite fabrication. A combination of PP (85 wt.%), SEBS (10 wt.%) and MA-g-SEBS (5 wt.%) was optimized and selected as the BM, similar to those used in the previous work [26, 28].

Results and discussion

ATR-IR

Table 1 depicts a summary of the ATR-IR spectra of FA showing the presence of a peak at 3477 cm^{-1} due to the adsorbed water (-OH group) of the montmorillonite in the FA [43]. Also, peaks at 1667 cm^{-1} [44], 1366 cm^{-1} [45], 1045 cm^{-1}[43, 46], and 778 cm^{-1} [47] confirm the presence of bond groups like C = O, N–O, Si–O-Si, and Si–C due to the mineral contents like organic matter, nitrate species, and quartz, respectively.

Similarly, for FA treated with silane coupling agent (APTES), two new peaks appeared at 2964 cm^{-1}, 2942 cm^{-1}, and 2863 cm^{-1} due to the presence of -CH$_3$ and -CH$_2$ and stretching vibration (Fig. 3a) [48–50]. Such peaks at 2964 cm^{-1}, 2942 cm^{-1}, and 2863 cm^{-1} correspond to the ethyl propyl group of the APTES, and hence, confirming the effective treatment by the APTES [48, 49]. Broadening in the

peaks at 1019 cm^{-1} and 798 cm^{-1} is due to the interaction and formation of Si–O-Si bonds and Si–O (from Si–OH) linkage from APTES and FA [51]. Peak at 1205 cm^{-1} corresponds to the stretching vibration of Si-CH$_3$ [52].

Figure 3b shows ATR-IR spectra of Ctab-treated FA indicating apparent omission and shifting of some peaks. These changes in ATR-IR spectra confirm possible interactions between the cationic surfactant Ctab and FA [53]. For instance, the peak at 3477 cm^{-1} is not visible in the Ctab-treated FA, which might be due to the breaking of the hydrogen bonds between adsorbed moisture from FA. The appearance of C-H stretching at 2970 cm^{-1} and 2856 cm^{-1} is due to the organic tail of the surfactant attached to FA, which may possibly improve its interaction with the matrix [53]. Peak broadening at 1038 cm^{-1} and 778 cm^{-1} might be due to the interaction between CTA$^+$ micelle and aluminosilicate in the FA. The presence of ionic interactions between cationic surfactant, Ctab, and FA particle was also presumed.

GO and CMC added in this study have been used as a secondary treatment for the APTES-treated FA. It is already well accomplished that GO is a very good carrier of FA. Larger surface area/unit mass ($\sim$ 2530 m^2/gm) and lamellar structure of GO is advantageous for carrying filler [54]. The new peaks for the GO-FA spectra around 1228 cm^{-1}, 1556 cm^{-1}, and 1652 cm^{-1} are due to the C–O–C stretching, N–H bending, and C = O stretching, respectively, confirming the presence of I, II and III amide linkage [29, 55] (Fig. 3c).

Similarly, CMC is also used as another carrier of the FA in this study. The CMC-FA hybrid spectra in Fig. 3d illustrate peaks at 3400 cm^{-1}, 1640 cm^{-1} (adsorbed water) and 1228 cm^{-1}, demonstrating the presence of NH-CO linkage in the CMC-hybridized FA [29, 55].

Table 1 Summary of results of ATR-IR spectra in terms of different frequencies corresponding to the different groups of the FA

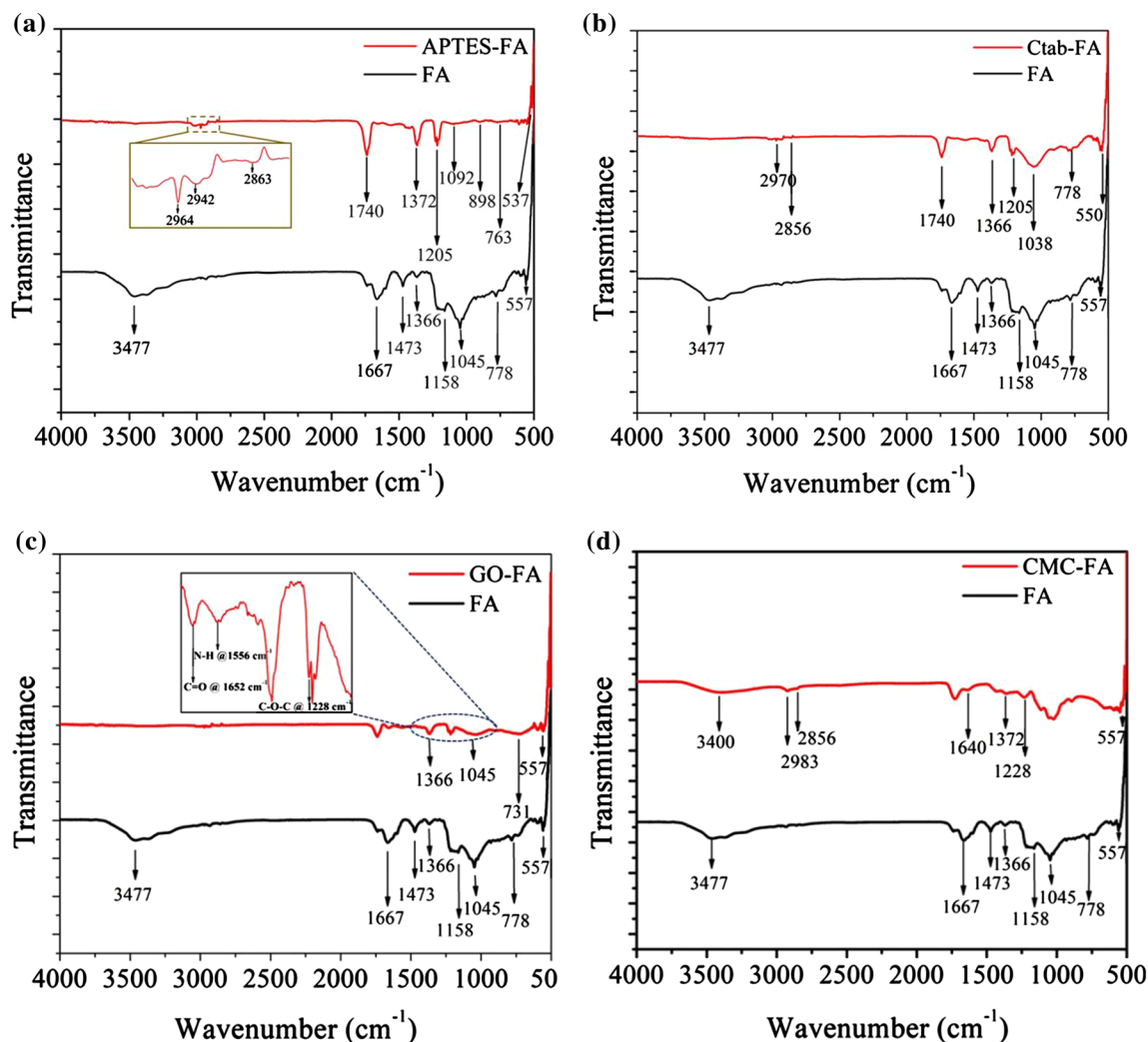| Frequency (cm^{-1})	Assigned group
3477	OH, adsorbed group of water due to stretching [43]
1667	Stretching vibration of C = O carboxylate group of organic matter [44]
1366	N–O stretching of nitrate species [45]
1045	Si–O-Si asymmetric stretching vibration [43, 46]
778	Si–O-Si symmetric stretching [47]

Figure 3 Diagram for the ATR-IR spectra of (a) APTES-treated FA (b) Ctab-treated FA (c) GO-hybridized FA (d) CMC-hybridized FA.

Interaction energy

The interaction energy among treated FA and MA-g-SEBS was evaluated using MD simulation protocols described earlier in "Matrix selection" section. The initial configurations of the systems considered for the simulation and those after equilibration have been presented in Fig. 4. The surface-treated FA: GO-FA, CMC-FA, and Ctab-FA were considered as one component, while MA-g-SEBS was considered as the other component in the whole system. Both the components were optimized separately and used to mimic a reinforcement–matrix interface. It was expected that MA part of the MA-g-SEBS would interact with the aluminosilicates of the treated and hybridized FA. The interaction energy, E_{IE} of each

system is calculated using Eq. (2) and the estimated values are listed in Table 2.

Likewise, it can be observed that the absolute value of E_{IE} was lowest (-5,280.96 kcal/mol) for Ctab-FA/MA-g-SEBS, which is indicative of a higher interaction at the interface compared to the other simulated systems, GO-FA/MA-g-SEBS and CMC-FA/MA-g-SEBS. In the MD simulation study, since there is no consideration of the formation or cleavage of any chemical bonds, and hence, the non-bonded interactions (comprising of E_{vdW} and $E_{Electrostatic}$) contribute majorly to the evaluated E_{IE}. In the present case, the van der Waals interaction among the nitrogen atom of Ctab and hydroxyl group of FA was more prominent in contrast to the interaction of silane-terminated FA with GO and CMC separately. The
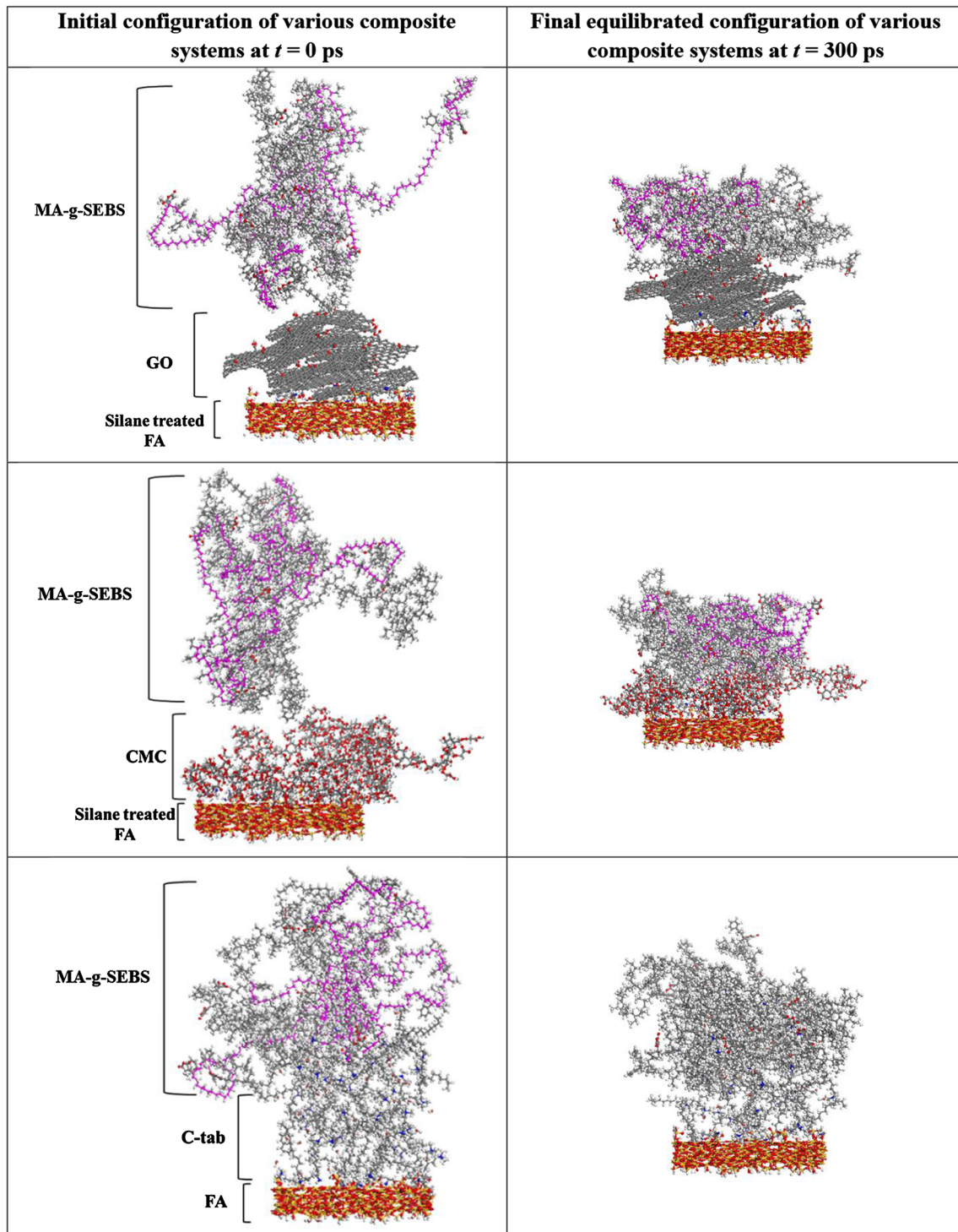
Initial configuration of various composite systems at *t* = 0 ps	Final equilibrated configuration of various composite systems at *t* = 300 ps

Figure 4 Configuration of the interface of different surface-treated FA/MA-g-SEBS systems before and after MD simulation run.

significance and the effect of this interfacial interaction are compared with the tensile strength of the composites in the latter part of the manuscript.

The possible reactions at the interface of reinforcement, MA-g-SEBS and APTES are presented in Scheme 2 for a better understanding.

Table 2 Interaction energy and different components of non-bond energies (all in kcal/mol) for different composite systems

System	E_{IE}	vdW	Electrostatic	Total non-bond
		(A)	(B)	(C = A + B)
GO-FA/MA-g-SEBS	116,574.92	1735.50	107,968.10	1,09,703.60
CMC-FA/MA-g-SEBS	113,917.35	908.80	1571.80	2480.60
Ctab-FA/MA-g-SEBS	− 5280.96	20,778.20	− 33,204.70	− 12,426.50

FE-SEM

The hybridization and reduction in particle size of FA reinforcement were studied by capturing FE-SEM images. Figure 5a and b depicts the FE-SEM capture of pristine FA and GO. FA particles and GO show the spherical and lamellar structure, respectively. This lamellar structure of the GO is advantageous for carrying out FA particles and produced a hybrid GO-FA reinforcement.

Likewise, the inset of Fig. 5c inspects that a few FA particles were situated on or favorably adhered to the surface of the GO. Also, Fig. 5d shows the presence of some flakes of GO over bigger particles of the FA. Both these figures evidently show a good hybridization between FA particles and GO flakes. The same appears to be in the case of CMC, shown in Fig. 5f, confirming FA particles adherence via strong chemical bonding (possibly amide linkage) on to the surface of the CMC, thereby increasing the surface roughness of the CMC fibers. The enhancement in the mechanical properties of the CMC-FA composite compared to PP might be due to the better surface roughness provided by these evenly distributed FA particles over the CMC surface. Moreover, as evident from Fig. 5g, h, Ctab-treated FA particles show a rough surface apparent from the grooves so formed. Hence, a combined effect of surface roughness and ionic bonding may lead to better interfacial interaction between treated FAs and polymer matrix. Likewise, Fig. 5i–k is fractured tensile samples of the composites. Figure 5i shows some broken FA and pulled CMC from the composite surface, thereby demonstrating a good transfer of the load from the matrix to the reinforcement. In the case of Ctab-FA-reinforced composite, good wetting of nanostructured FA makes composite stronger, and hence, as a result, increased mechanical properties have been reported (Fig. 5j). However, GO-FA-reinforced composites in Fig. 5k showed that the GO-FA particles

were not completely embedded within BM. Also, the presence of unbroken FA on composite surface shows evidence of relatively poor interfacial interactions.

Mechanical properties

Tensile strength

The tensile strength of the pristine PP (30.61 MPa), BM (27.52 MPa) and their composites are presented in Table 3. It was observed that CMC-FA and Ctab-FA reinforcement improved the tensile strength and showed a value of 34.63 MPa and 32.76 MPa, respectively. Using BM as the matrix in the composites, increased the tensile strength since the interfacial interaction among coupling agent MA-g-SEBS and treated/hybridized FA improved. Both treatment/hybridization of FA and presence of MA group of MA-g-SEBS [56] in BM play an important role in improving interfacial adhesion. Likewise, CMC-FA and Ctab-FA incorporation into the composites increased the tensile strength of the composites by $\sim$ 13% and $\sim$ 7% in comparison with PP. FA hybridized CMC has a better interaction to polymer due to increased mechanical roughness on the CMC surface (Fig. 5f). Furthermore, -OH group at CMC surface also interacts with the MA group of the MA-g-SEBS of BM, forming a strong ester and hydrogen bond. Likewise, Ctab-treated FA has a long tail of organic chain group, which interacts with the polymer BM and forms a bridge between FA and BM. It is worth noting here that due to the continuous high energy ball milling, significant and benign reduction in the FA particle size was achieved. This nano-sized FA particles are more reactive and available for interaction with matrix than pristine FA so as to overall improve the tensile strength of the composites. Hence, a larger surface area offered by nano-sized FA and increased surface roughness lead to enhanced mechanical interlocking with BM
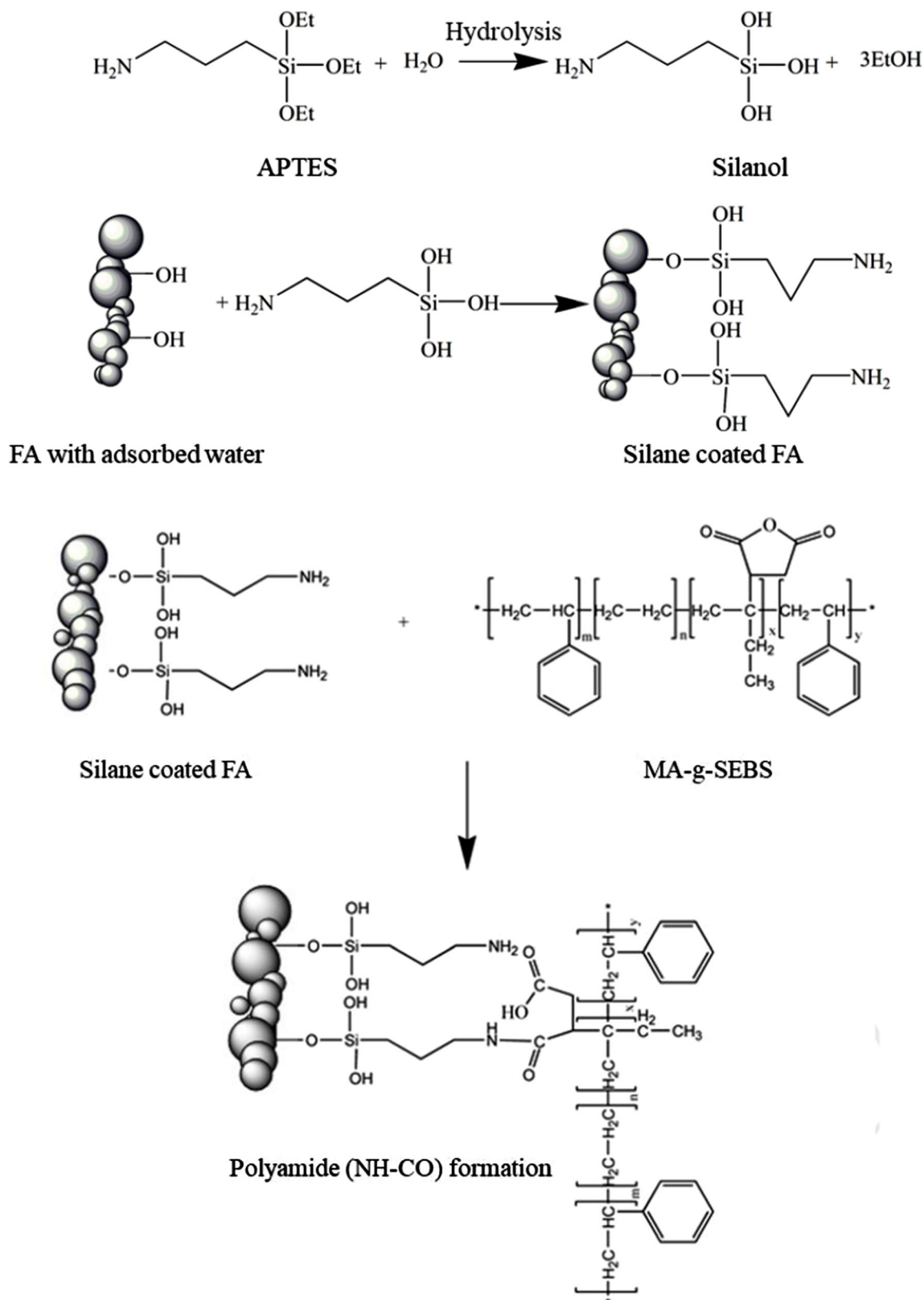
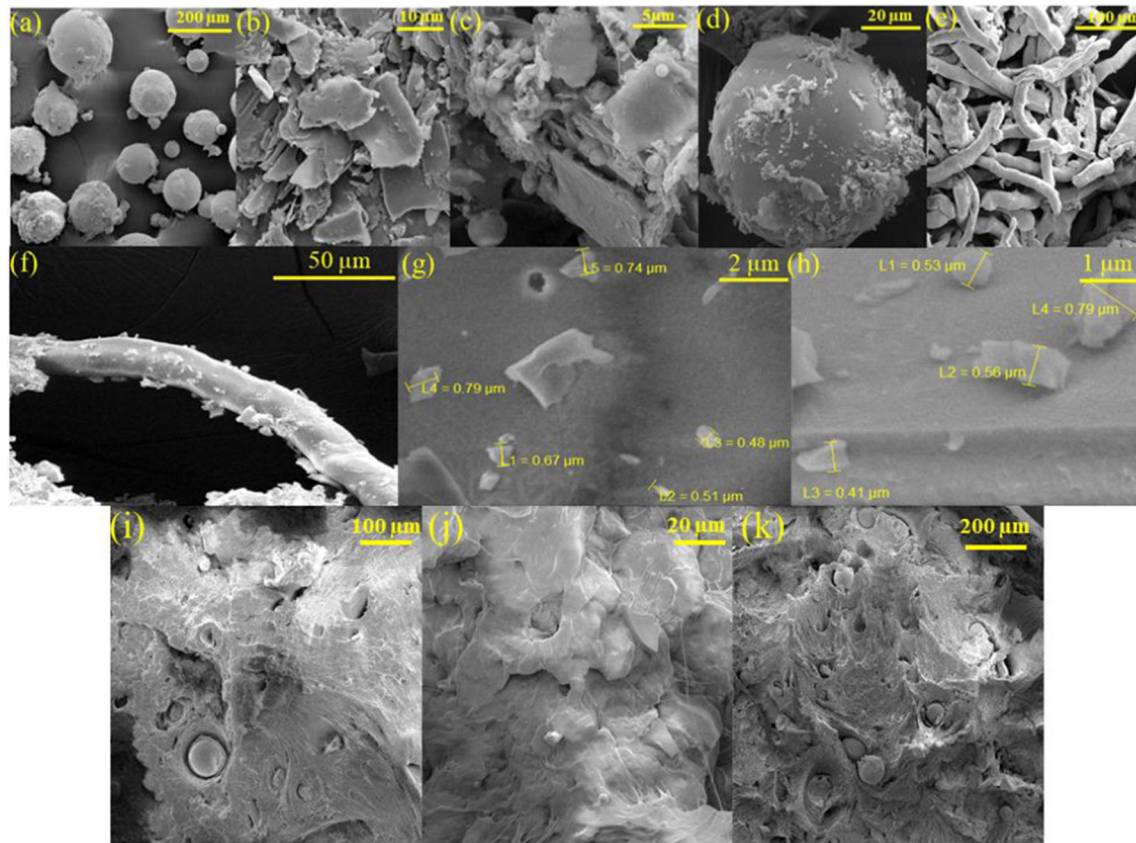**Scheme 2** The possible reactions among the silanol and MA group of BM.

Figure 5 Interpretation of FE-SEM images showing (**a**) FA particles (**b**) GO flakes (**c**) FA particles carried over GO (**d**) GO-coated FA (**e**) CMC (**f**) FA particles carried over CMC (**g**, **h**) Ctab-treated FA (**i**) CMC-FA composite (**j**) Ctab-FA composite (**k**) GO-FA composite.

Table 3 Tensile toughness of the pure polypropylene, BM, and composites fabricated from hybrid and treated FA

Samples	Tensile strength (MPa)	Tensile modulus (GPa)	Tensile toughness (MJ/m^3)	Elongation at break (%)	Flexural strength (MPa)	Flexural modulus (GPa)	Shore D hardness
PP	30.61	1.01	13.14	60.00	35.86	1.00	59
BM	27.52	0.73	14.41	80.26	26.24	0.73	55
CMC-FA	34.63	1.08	12.12	53.30	46.46	2.03	61
Ctab-FA	32.76	1.04	9.70	43.60	44.82	1.80	70
GO-FA	24.54	0.80	5.13	27.28	42.00	1.53	67

culminating in effective load transfer from matrix to reinforcement [57]. Additionally, electrostatic bond interaction between Ctab-FA and MA-g-SEBS showed highest bond energy (Table 2). Table 3 shows that in the case of the GO-FA composites, tensile strength decreased compared to BM and PP due to the relatively less effective load transfer from the BM to FA. This is despite that there was good adhesion

between GO and silane-treated FA confirmed by ATR-IR and FE-SEM analysis, in "Interaction energy" and "Mechanical Properties" sections, respectively [54]. But the interaction between GO-FA hybrid and BM does not show any effective load transfer due to insignificant interfacial adhesions.

However, 5 wt.% of untreated FA and treated with tri-methoxy propyl silane and APTES was reinforced

in PP by Doddipatla et al. [58]. All three types of treated/untreated FA-reinforced composites reported a reduced tensile strength compared to the base matrix PP [58]. Likewise, composite prepared with 20 phr polyolefin elastomer, 5 phr PP-g-MA, 5 phr FA and PP reported very marginal increase in the tensile strength (30.78 MPa) compared to PP (30.05 MPa) [59].

Also, Das et al. [60] reinforced 5 wt.% of cenosphere to the PP and found the tensile stress less than the base matrix. This study also confirms that the mechanism of deformation is insubstantially affected by the loading up to 10 wt.% of FA loading and fracture behavior is controlled by base matrix/PP [60]. In another study, Chand et al. [61] reinforced 5 wt.% of FA in the blend of PP/PMMA (80:20) and reported the same inferior tensile stress property compared to blend base matrix.

The tensile modulus, which is the elastic regime of the stress–strain response of the composites prior to failure/fracture (Table 3) of all the composites, is found to be increased compared to BM (0.73 GPa). However, only CMC-FA (1.08 GPa)- and Ctab-FA (1.04 GPa)-reinforced composites exhibited tensile modulus higher than PP (1.01 GPa) due to better physical resistance offered by the reinforcements against the external load application. The decrease in tensile modulus of GO-FA (0.8 GPa)-reinforced composite might be attributable to the less resistance offered by reinforcement against an external load application. However, the tensile modulus of all the composites were superior than BM followed slight improvement by GO-FA composite. The same marginal improvement was reported by various researchers on adding 5 wt.% of FA to the base matrix [58–61]. An increase in elastic modulus but the decrease in tensile strength of the composite may be explained since the modulus is correlated to the elastic regime of the stress–strain response prior to failure or fracture. Whereas, the tensile strength of the composites associated with the load transfer, hence, as result of interaction among interfaces of reinforcement and base matrix plays an important role [60].

This decrease in modulus in GO-FA has been confirmed from a lower interaction captured through the higher positive value of interaction energy calculated using the MD simulations (see "FE-SEM" section), thereby highlighting lower interactions among components. Also, the lowest interaction

energy (highest bond energy) calculated from the simulation was recorded for the Ctab-FA composite compared to CMC-FA composite, which is contradictory to the corresponding experimental tensile strength values of the composite. This might be due to the strong ester and hydrogen bond formation between the -OH group of the CMC and of MA-g-SEBS. Additionally, a lower value of electrostatic interactions was recorded for the CMC-FA composites in comparison with Ctab-FA. Also, lesser theoretical bond energy reported in the CMC-FA system might be attributable to the least FA content used in the CMC-FA composite due to the coating of the FA on the CMC surface. From Table 2, it was also demonstrated that electrostatic forces acting within Ctab-FA-reinforced composite was more prominent compared to CMC-FA and GO-FA system. Interestingly, in the experimental calculation highest tensile strength of 34.63 MPa was recorded for CMC-FA-reinforced composite. This contradiction depicts that the simultaneous effect of chemical interaction (covalent bonding) and van der Waals interactions (Table 2) between the interfaces is more prominent than only electrostatic one. It was also worth noting that Ctab: FA ratio was 100:6 in Ctab-FA during treatment, unlike CMC-FA and GO-FA, which used a 50:50 of CMC and GO wt.% with FA, respectively. Likewise, for GO-FA-reinforced composites, none of the physical or chemical interactions were found significant and reported the lowest tensile strength of 24.54 MPa. Hence, the lowest interaction energy, tensile strength, and tensile modulus were recorded for the GO-FA. It may be noted that the interaction energy estimates reported for all the composites from MD simulation do not include covalent interactions.

Tensile toughness and elongation at break

Tensile toughness of the pure polypropylene, BM, and composites have been reported by calculating the area under the tensile stress–strain curves presented in Fig. 6 (Table 3). The lowest and highest toughness values of 13.14 MJ/m^3 and 14.41 MJ/m^3 have been shown by pure PP and BM, respectively (Table 3). It is also to be noted that the toughness value of all the composites falls lower than the toughness value of pure PP and BM. This apparent decrease in the toughness was due to the addition of the reinforcing FA in BM. Besides, CMC-FA and Ctab-FA composites showed a tensile strength more than pure PP with 5
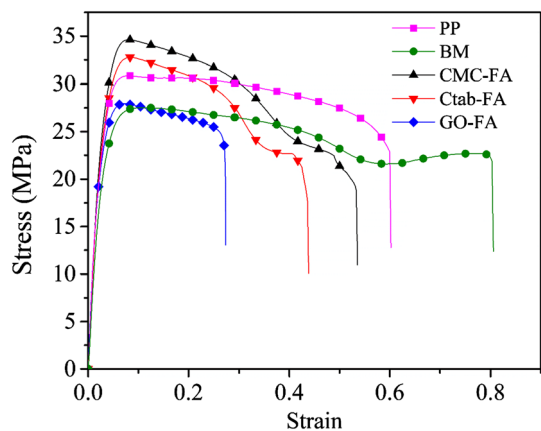
Figure 6 Illustration of the tensile stress vs strain curve of the PP, BM, CMC-FA, Ctab-FA, and GO-FA.

wt.% of hybridized or treated FA and having BM as the base matrix. Thus, a positive effect of using hybridized FA and treated FA with SEBS and MA-g-SEBS on impact and tensile strength is evident. It is also to be noted that the addition of FA shows opposite effects on both the toughness and tensile strength of the composites. However, an increase in the tensile strength of the composites has been achieved at the cost of some decrease in the impact strength and toughness of the composites (Fig. 7).

Furthermore, in the composites CMC-FA, Ctab-FA, and GO-FA, the elongation at break decreased relative to PP by approximately $\sim$ 11%, $\sim$ 27%, and $\sim$ 55%, respectively.

Among these samples, CMC-FA, Ctab-FA, and GO-FA have shown both tensile toughness and elongation at break lower than that of pure PP attributable to the presence of hybridized and
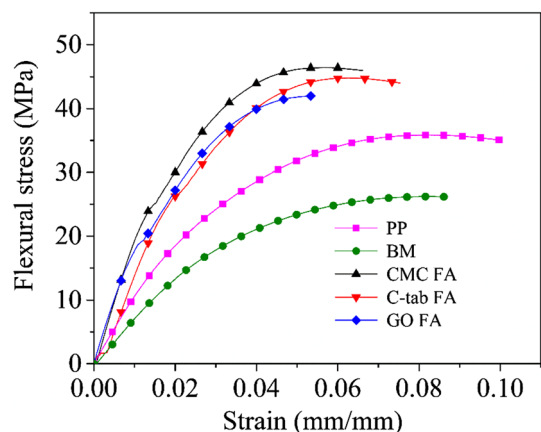

Figure 7 Illustration of the flexural stress versus strain curve of the PP, BM, CMC-FA, Ctab-FA, and GO-FA composites.

reinforcing FA in the BM. GO-FA-incorporated BM composites showed a higher decrease in toughness and also failed at tensile strength, which might be due to the increasing FA-FA interaction [62]. The highest elongation at break of 80.26% has been shown by BM in comparison with PP. Among, all reinforcement CMC-FA incorporation leads to the highest elongation at break in comparison with GO-FA and Ctab-FA composites. The highest toughening value of the CMC-FA may be attributable to the lowest FA and CMC content since it was prepared in 50:50 wt.% (CMC: FA).

As per data reported by Doddipatla et al. [58], toughness and elongation at break of the 5 wt.% reinforced polypropylene composite increase with an increase in the interfacial adhesion. Composite made of 5 wt.% of FA treated with TMPS showed highest tensile toughness and elongation at break.

Flexural Strength

Flexural strength of PP, BM and all the samples of composites have been reported in Table 3. Interestingly, incorporation of treated/hybridized FA into the BM enhanced the flexural strength of all the composites compared to PP. CMC-FA-, Ctab-FA-, and GO-FA-incorporated polymer composites showed a flexural strength (46.46 MPa, 44.82 MPa, and 42.00 MPa) higher than that of the pristine PP (35.86 MPa). The flexural strength of the composite fabricated by incorporating CMC-FA shows the highest value, while the one incorporated with GO-FA showed the lowest. Presumably, the formation of strong ester and hydrogen bong between -OH group of CMC and MA group of BM granted effective load transfer from matrix to reinforcement [63]. On the other hand, long tail of the organic part of Ctab interacts with the BM provides a good interaction. Also, the small size of FA ($\sim$ 800 nm) providing effective reactive and large specific surface area, which helps in interacting favorably with BM. Unlike, tensile strength there is an apparent increase in flexural strength of GO-FA incorporated composites compared to pristine PP still, the observed increase was less than that for case of CMC-FA and Ctab-FA-reinforced composites. This increase in flexural strength might be due to the load bearing capacity of GO in a composite. The flexural modulus (Table 3) of entire range of composites displayed an improved value, where the most excellent flexural modulus of

2.03 GPa was possessed by CMC-FA-based composite. This improvement in the flexural modulus was exhibited due to the good resistance offered against the external load by the treated and hybridized FA, in the BM. The flexural strength of Ctab-FA (1.80 GPa)-filled BM lay in between the flexural modulus values of CMC-FA and GO-FA (1.53 GPa)-filled composites. The above results confirm that the addition of a stiffer reinforcements to the BM lead to the increment in the modulus values of the composites. However, composite fabricated from 20 phr POE, 5 phr PP-g-MA, 5 phe untreated FA and PP showed an increment from 39.41 MPa to 41.64 MPa which was still lesser than all the composite prepared in the current study [59]. Likewise, 5 wt.% cenospheres filled PP showed decreased flexural strength and increased flexural modulus, indicating although rigidity was improved but resistance against bending was not enough [60]. This might be again due to the insubstantial adhesion among reinforcement and BM.

Shore D hardness

A shore D hardness value of PP, BM and all the composites have been summarized in Table 3. PP demonstrated a shore D hardness value of 59. Incorporation of SEBS and SEBS-g-MA to the PP decreased the hardness value of BM (55) compared to PP. However, due to the inclusion of hard and stiff FA (due to its ceramic nature) in the composite system shore D hardness value of all the composites were found to increase. Similar increase in hardness with fillers addition to PP was also earlier reported by Gogoi et al. which is in agreement of the current study [63]. Highest hardness and lowest values of 70 and 61 were recorded for Ctab-FA- and CMC-FA-reinforced composite. GO-FA-reinforced composite possessed a shore D value of 67.

Thermal Properties

DSC

Thermal study of the composites has been performed by the differential scanning calorimetry by first heating samples from 25 °C up to 250 °C to remove the thermal history followed by cooling up to -60 °C and second heating up to 250 °C. Samples were tested in the low temperature range (up to -60 °C) to check the thermal behavior before (glassy region) and

after (rubbery region) glass transition temperature (T_g) of the composites, which was presumed to be around -10 °C [64]. Figure 8 interprets the endothermic and exothermic curves of PP, BM, and different composites. Melting temperature (T_m) from endothermic and crystallization temperatures (T_c) temperature from exothermic peaks can be determined. T_m, T_c, melting enthalpy (ΔH), and percentage crystallinity (X_c) of all the samples have been reported in Table 4.

Various crystallographic phases of PP have been reported earlier by Sengupta et al. [65]. The thermodynamically α-monoclinic is the most stable phase of the PP. Melting of this phase recorded at 164.81 °C reported in our previous study [26]. An insignificant difference of ∼ 3 °C in the T_m of the composites compared to that of PP shows that the reinforcements do not affect the melting behavior of PP. Additionally, BM reflects a minor change in the melting behavior (165 °C). The heterogeneous nucleating effect of the reinforcements resulted in a higher shift of the exothermic curve (T_c) of the composites by 3–4 °C. Probably, reinforcements must have accelerated the rate of crystallization at higher temperatures [63]. Likewise, the highest acceleration in the rate of crystallization was exhibited for the Ctab-FA-reinforced composite, and it was presumed that the small particle size of Ctab-FA might have promoted the same. Table 4 lists the values of T_c, T_m, ΔH, and %X_c for PP, BM, and composites. 70.20% of X_c was reported for pristine PP. The addition of elastomeric phase in the form of SEBS and MA-g-SEBS to the PP reduces the crystallinity of the BM further to 43.18%. Likewise, the crystallinity of the composite increases
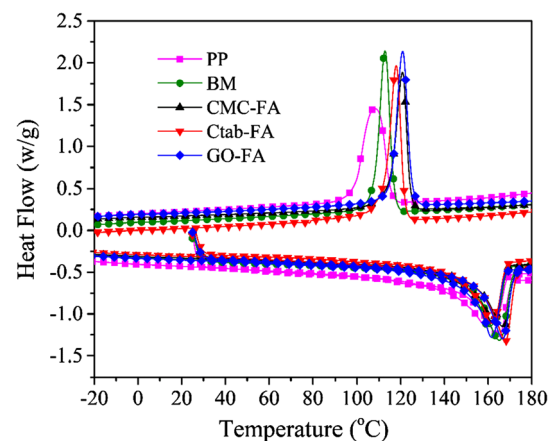
Figure 8 Illustration of the thermograms of the PP, BM, CMC-FA, Ctab-FA, and GO-FA composites.

Table. 4. Values of T_c, T_m, ΔH, and $\%X_c$ for pristine PP, BM, and composites

Samples	T_c(°C)	T_m(°C)	ΔH (J/g)	$\%X_c$
PP*	107.80	164.81	146.73	70.20
BM*	112.77	165.13	90.249	43.18
CMC-FA	120.80	167.27	105.04	50.38
Ctab-FA	117.91	167.65	128.30	61.24
GO-FA	120.80	166.61	70.91	33.92

*DSC data of PP and BM both reported here are from our previous study[26]

with the addition of CMC-FA (50.38%) and Ctab-FA (61.24%) reinforcement to the BM. A high crystallization rate exhibited due to the reinforcement particles was the reason behind enhanced crystallinity. This result was in agreement with Gogoi et al., and the author reported an increase in crystallinity of the composite due to the addition of a hollow glass microsphere and natural fiber to the PP [63].

Also, the incorporation of GO-FA to the composites decreases the crystallinity of the BM further to 33.92%. This drop-in crystallinity might be attributable to the disturbance created by the GO-FA hybrid particles in between the chain regularity of BM and PP. Appropriate interactions between GO-FA and BM might have been a reason for a significant drop-in crystallinity. A similar study has been reported by Sengupta et al. [65]. Earlier where melting enthalpy (ΔH) as a result of crystallinity was found to drop due to the incorporation of FA to the recycled polypropylene. Gogoi et al. [63] also reported a decrease in crystallinity due to the incorporation of hollow glass microspheres to the polypropylene matrix. The authors reported that as HGM content increases, reinforcement surface per unit area also increases and interaction between PP and HGM takes place via PP-g-MA. This good interaction although accelerates the crystallization rate but the presence of reinforcement creates a hindrance in the crystal growth and ultimately disrupts the crystallinity. In the GO-FA-incorporated polymer composite, GO, being a good carrier, provides a good surface for FA and matrix interaction and, hence, creates hindrance in the crystal growth of the matrix in the composites.

It is also evident from the earlier reports that the addition of FA/cenosphere may increase or decrease

the crystallinity of the composites. For instance, 5 wt.% of FA-filled PP/PMMA (80:20) composite decreases the crystallinity [60, 61]. However, with the same wt.% of FA Yao et al. reported an improved crystallinity of the composites [59]. Precisely, crystallization of the composite may increase /decrease depending on the nucleation and crystal growth of the BM. More inhibition to the polymeric chain arrangement surely will lead to a decreased crystallinity.

TGA

The TGA graphs of PP, BM, FA, and composites are presented in Fig. 9. Degradation peaks and behavior of all the composites show resemblance with that of PP and BM with only slight changes in the degradation temperature. Release of volatiles was recorded on initial heating of the FA due to the presence of unburnt carbon, waxes, etc. The degradation temperature of different samples corresponding to 5 (T_i), 50 (T_{50}), 75 (T_{75}), and more than 90% (T_{max}) weight loss has been reported in Table 5. PP shows T_i, T_{50}, T_{75}, and T_{max} at 295, 378, 398, and 413 °C, respectively. FA releases volatiles in small concentration up to 512 °C due to the presence of unburnt carbons, waxes etc. It has been observed that there was a negligible change in behavior of the degradation temperature up to 5 wt.% loss of PP, BM, and all the composites. 5 wt.% loss of the samples has been observed for PP at 295 °C, BM at 287 °C, CMC-FA at 277 °C, Ctab-FA at 274 °C, and GO-FA at 286 °C (Table 5). As temperature increases, the thermal stability of the PP decreases in comparison with BM and
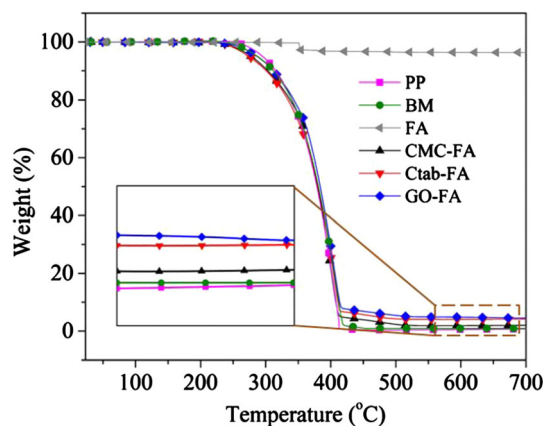

Figure 9 Thermogravimetric analysis (TGA) plots of PP, BM, FA, CMC-FA, Ctab-FA, and GO-FA composites.

Table 5 Depiction of degradation behavior taken from TGA analysis of composites and its constituents at different percentages of wt. loss

Sample	T_i (°C)	T_{50} (°C)	T_{75} (°C)	$T_{max.}$ (°C)
PP	295	378	398	413
FA	512	NA	NA	NA
BM	287	380	401	419
CMC-FA	277	380	397	413
Ctab-FA	274	379	400	415
GO-FA	286	383	402	417

T_i: initial degradation temperature at 5 wt.% loss, T_{50}: temperature at 50 wt.% loss, T_{75}: the temperature at 75 wt.% loss, $T_{max.}$: degradation temperature at maximum wt.% loss

all the composites. An increase in thermal stability of BM at higher temperatures is exhibited, which is attributed to the styrene component of SEBS and MA-g-SEBS. GO-FA, which constitutes graphene oxide-hybridized FA and 95 wt.% of BM, demonstrated maximum heat stability and degradation temperature was highest at all the wt.% sample loss among all the composites. This increase in the thermal stability of GO-FA has been attributed to the high degradation temperature of graphene oxide. Composites CMC-FA, Ctab-FA, and BM showed temperatures of degradation (after the 5 wt.% loss) in between those of PP and GO-FA composite. Noticeably, the thermal degradation temperature of the fabricated composites surged to a higher temperature upon the addition of FA corresponding to 50 and 75 wt.% loss. Subsequently, the entire degradation process ends at ∼ 800 °C, and the residual mass left by FA and PP were 97% and 0.66%. There were no noticeable volatile materials have been found in the composites CMC-FA, Ctab-FA, and GO-FA (Fig. 9). The weight of the residuals at 800 °C for BM, FA, CMC-FA, Ctab-FA, and GO-FA, composites were found to be in between the residual mass of PP and FA and values were 0.9 wt.%, 96.52 wt.%, 1.93 wt.%, 4.09 wt.%, and 4.65 wt.%, respectively.

With the addition of the 5 wt.% of FA/ cenosphere, almost all the composites showed single-step degradation and increased thermal degradation temperature at all temperatures. Increments in the char wt.% have also been reported due to the presence of burnt FA inorganic/impurities in the composites [59–61]. FA hardly showed any sign of decomposition/melting before 800 °C; hence, as a result, it slows down

the decomposition and evaporation of pyrolytic gaseous products by forming an insulating layer in the composite [66].

DTG

DTG curves of all the samples have been represented in Fig. 10. There was a very negligible difference between the temperature of initiation of degradation and final degradation. Sample PP, BM and all the composites showed the highest rate of degradation in the range of between 405–410 °C. PP showed the highest rate of degradation at 405 °C followed by BM at around 404 °C. All the composites possessed some stability compared to PP and BM and a decrease in rate of degradation has been observed. Composite incorporated with CMC-hybridized FA was least stable in comparison with composites fabricated from Ctab-treated FA and GO-hybridized FA. A decrease in thermal stability of CMC-FA composite is perhaps exhibited due to the existence of CMC onto FA. CMC takes extensive disintegration in the span of 320–500 °C that is analogous to cellulose which is lower than that of FA [67]. Likewise, GO is thermally most stable after FA among all the reinforcements and composites, and hence, the lowest rate of degradation has been exhibited by GO-FA composites.

Conclusion

Treated and hybridized FA reinforcements incorporated impact-modified PP composites were successfully prepared, tested, and characterized in this
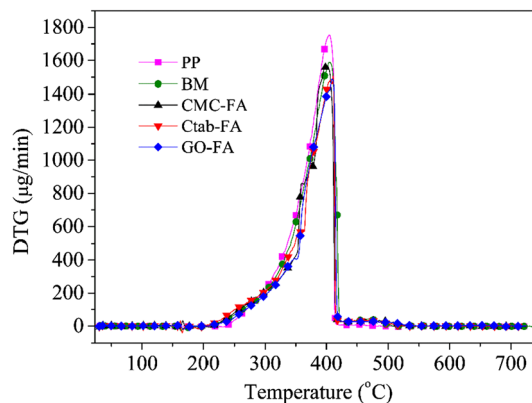

Figure 10 DTG curves for PP, BM, CMC-FA, Ctab-FA, and GO-FA composites.

study. An improved mechanical and thermal (stability) properties were reported for CMC-FA- and Ctab-FA-reinforced composites compared to PP. This positive shift in both these properties must have been exhibited due to the strong interfacial interactions among reinforcements and BM. CMC-hybridized FA and Ctab-treated FA demonstrated the most significant improvement of $\sim$ 13% and $\sim$ 7% in the tensile strength compared to PP. An improvement of $\sim$ 17% by GO-FA- , $\sim$ 25% by Ctab-FA- , and $\sim$ 30% by CMC-FA-reinforced composites were reported compared to PP in the flexural strength. FE-SEM images of the composites shown that treated/hybridized FA particles were fully adhered with BM and good interaction was evident. Thermogram (DSC) reads an insignificant difference of $\sim$ 3 °C in all the composites compared to pristine PP, confirming that the incorporation reinforcements do not affect the melting behavior much. Additionally, the 3–4 °C shifting in the exothermic curve or higher T_c for all the composites might be exhibited due to the heterogeneous nucleating effect of the differently treated/hybridized FA, which might have accelerated the crystallization rate at higher temperatures. Thermogravimetric (TGA) study reports a probable improvement in the thermal degradation temperature of all the composites due to the addition of burnt FA compared to pristine PP, especially at 50 and 75 wt.% loss. MD simulations were used to predict the interfacial adhesion and binding energy among reinforcing material and polymer matrix. While the simulations provided the strongest non-bonded interaction between Ctab and BM among all reinforcements, the experimentally determined properties indicated improved properties for CMC-FA-based composites. The above-discussed results showed that by controlling interfacial interactions at the interface of FA and base matrix, various properties of the composites could be improved significantly and such use of FA could be an evolutionary step toward FA management issue faced by societies.

Acknowledgements

Declaration

References

[1] Tongia R, Gross S (2019) Coal in India: Adjusting to transition

[2] Yousuf A, Manzoor SO, Youssouf M et al (2020) Fly ash: production and utilization in India-an overview. J Mater Env Sci 11:911–921

[3] Yang S, Tian J, Bian X, Wu Y (2020) High performance NBR/fly ash composites prepared by an environment-friendly method. Compos Sci Technol 186:107909. https://doi.org/10.1016/j.compscitech.2019.107909

[4] Choi SK, Lee S, Song YK, Moon HS (2002) Leaching characteristics of selected Korean fly ashes and its implications for the groundwater composition near the ash disposal mound. Fuel 81:1083–1090. https://doi.org/10.1016/S0016-2361(02)00006-6

[5] Sushil S, Batra VS (2006) Analysis of fly ash heavy metal content and disposal in three thermal power plants in India. Fuel 85:2676–2679. https://doi.org/10.1016/j.fuel.2006.04.031

[6] Jain M (2014) Dwivedi A (2014) Fly ash – waste management and overview: A Review Fly ash – waste management and overview: A Review. Recent Res Sci Technol 6(1):30–35

[7] Patra KC, Rautray TR, Nayak P (2012) Analysis of grains grown on fly ash treated soils. Appl Radiat Isot 70:1797–1802. https://doi.org/10.1016/j.apradiso.2012.03.037

[8] Nyale SM, Eze CP, Akinyeye RO et al (2014) The leaching behaviour and geochemical fractionation of trace elements in hydraulically disposed weathered coal fly ash. J Environ Sci Heal - Part A Toxic/Hazardous Subst Environ Eng 49:233–242. https://doi.org/10.1080/10934529.2013.838929

[9] Wong J (1995) The production of artificial soil mix from coal fly ash and sewage sludge. Environ Technol (United Kingdom) 16:741–751. https://doi.org/10.1080/09593331608616313

[10] Su DC, Wong JWC (2002) The growth of corn seedlings in alkaline coal fly ash stabilized sewage sludge. Water Air Soil Pollut 133:1–13. https://doi.org/10.1023/A:1012998530689

[11] Jiang RF, Yang CG, Su DC, Wong JWC (1999) Coal fly ash and lime stabilized biosolids as an ameliorant for boron deficient acidic soils. Environ Technol (United Kingdom) 20:645–649. https://doi.org/10.1080/09593332008616860

[12] Querol X, Moreno N, Umaña JC, Alastuey A et al (2002) Synthesis of zeolites from coal fly ash: an overview. Int J coal Geol 50:413–423

[13] González A, Navia R, Moreno N (2009) Fly ashes from coal and petroleum coke combustion: current and innovative potential applications. Waste Manag Res 27:976–987

[14] Erol M, Küçükbayrak S, Ersoy-Meriçboyu A (2008) Characterization of sintered coal fly ashes. Fuel 87:1334–1340. https://doi.org/10.1016/j.fuel.2007.07.002

[15] Bhattacharjee U, Kandpal TC (2002) Potential of fly ash utilisation in India. Energy 27:151–166. https://doi.org/10.1016/S0360-5442(01)00065-2

[16] Wang S (2008) Application of solid ash based catalysts in heterogeneous catalysis. Environ Sci Technol 42:7055–7063

[17] Yang S, Tian J, Bian X, et al High performance NBR/fly ash composites prepared by an environment-friendly method. Elsevier

[18] Sengupta S, Ray D, Mukhopadhyay A (2013) Sustainable materials: Value-added composites from recycled polypropylene and fly ash using a green coupling agent. ACS Sustain Chem Eng 1:574–584. https://doi.org/10.1021/sc3000948

[19] Sengupta S, Pal K, Ray D, Mukhopadhyay A (2011) Furfuryl palmitate coated fly ash used as filler in recycled polypropylene matrix composites. Compos Part B Eng 42:1834–1839. https://doi.org/10.1016/j.compositesb.2011.06.021

[20] Sridhar V, Xiu ZZ, Xu D et al (2009) Fly ash reinforced thermoplastic vulcanizates obtained from waste tire powder. Waste Manag 29:1058–1066. https://doi.org/10.1016/j.wasman.2008.08.013

[21] Kuźnia M, Magiera A, Pielichowska K et al (2019) Fluidized bed combustion fly ash as filler in composite polyurethane materials. Waste Manag 92:115–123. https://doi.org/10.1016/j.wasman.2019.05.012

[22] Goh CK, Valavan SE, Low TK, Tang LH (2016) Effects of different surface modification and contents on municipal solid waste incineration fly ash/epoxy composites. Waste Manag 58:309–315. https://doi.org/10.1016/j.wasman.2016.05.027

[23] Yang S, Liang P, Hua K et al (2018) Preparation of carboxylated nitrile butadiene rubber/fly ash composites by in-situ carboxylate reaction. Compos Sci Technol 167:294–300. https://doi.org/10.1016/j.compscitech.2018.08.007

[24] Yang S, Liang P, Peng X et al (2018) Improvement in mechanical properties of SBR/Fly ash composites by in-situ grafting-neutralization reaction. Chem Eng J 354:849–855. https://doi.org/10.1016/j.cej.2018.08.112

[25] Bharath Kumar BR, Doddamani M, Zeltmann SE et al (2016) Effect of particle surface treatment and blending method on flexural properties of injection-molded cenosphere/HDPE syntactic foams. J Mater Sci 51:3793–3805. https://doi.org/10.1007/s10853-015-9697-2

[26] Maurya AK, Gogoi R, Manik G (2021) Mechano-chemically activated fly-ash and sisal fiber reinforced PP hybrid composite with enhanced mechanical properties. Cellulose. https://doi.org/10.1007/s10570-021-03995-4

[27] Filho AS, Parveen S, Rana S et al (2021) Micro-structure and mechanical properties of microcrystalline cellulose-sisal fiber reinforced cementitious composites developed using cetyltrimethylammonium bromide as the dispersing agent. Cellulose. https://doi.org/10.1007/s10570-020-03641-5

[28] Maurya AK, Gogoi R, Manik G (2021) Study of the Moisture Mitigation and Toughening Effect of Fly-ash Particles on Sisal Fiber-Reinforced Hybrid Polypropylene Composites. J Polym Environ. https://doi.org/10.1007/s10924-021-02043-3

[29] Pettignano A, Charlot A, Fleury E (2019) Solvent-Free Synthesis of Amidated Carboxymethyl Cellulose Derivatives: Effect on the Thermal Properties. Polymers (Basel) 11:1227. https://doi.org/10.3390/polym11071227

[30] Joseph S, Bambola VA, Sherhtukade VV, Mahanwar PA (2011) Effect of flyash content, particle size of flyash, and type of silane coupling agents on the properties of recycled poly (ethylene terephthalate)/flyash composites. J Appl Polym Sci 119:201–208

[31] Gogoi R, Manik G (2021) Development of thermally conductive and high-specific strength polypropylene composites for thermal management applications in automotive. Polym Compos 42:1945–1960. https://doi.org/10.1002/pc.25947

[32] Gogoi R, Manik G, Arun B (2019) High specific strength hybrid polypropylene composites using carbon fibre and hollow glass microspheres: Development, characterization and comparison with empirical models. Compos Part B Eng 173:106875. https://doi.org/10.1016/j.compositesb.2019.05.086

[33] Cui YH, Wang XX, Li ZQ, Tao J (2010) Fabrication and properties of nano-ZnO/glass-fiber-reinforced polypropylene composites. J Vinyl Addit Technol 16:189–194. https://doi.org/10.1002/vnl.20231

[34] Material StudioTM, by Dassault Systemes BIOVIA, UK (Accelrys®), License purchased by IIT Roorkee.

[35] Gogoi R, Sethi SK, Manik G (2021) Surface functionalization and CNT coating induced improved interfacial interactions of carbon fiber with polypropylene matrix: a molecular dynamics study. Appl Surf Sci. https://doi.org/10.1016/j.apsusc.2020.148162

[36] Sethi SK, Manik G (2018) Recent progress in super hydrophobic/hydrophilic self-cleaning surfaces for various industrial applications: a review. Polym Plast Technol Eng 57:1932–1952. https://doi.org/10.1080/03602559.2018.1447128

[37] Nosé S (1984) A unified formulation of the constant temperature molecular dynamics methods. J Chem Phys 81:511–519. https://doi.org/10.1063/1.447334

[38] Sethi SK, Singh M, Manik G (2020) A multi-scale modeling and simulation study to investigate the effect of roughness of a surface on its self-cleaning performance. Mol Syst Des Eng 5:1277–1289. https://doi.org/10.1039/d0me00068j

[39] Sethi SK, Soni L, Shankar U et al (2020) A molecular dynamics simulation study to investigate poly(vinyl acetate)-poly(dimethyl siloxane) based easy-clean coating: An insight into the surface behavior and substrate interaction. J Mol Struct 1202:127342. https://doi.org/10.1016/j.molstruc.2019.127342

[40] Sethi SK, Manik G (2021) A combined theoretical and experimental investigation on the wettability of MWCNT filled PVAc-g-PDMS easy-clean coating. Prog Org Coatings 151:106092. https://doi.org/10.1016/j.porgcoat.2020.106092

[41] Sharma R, Maiti SN (2014) Effects of crystallinity of PP and flexibility of SEBS-g-MA copolymer on the mechanical properties of PP/SEBS-g-MA blends. Polym - Plast Technol Eng 53:229–238. https://doi.org/10.1080/03602559.2013.843706

[42] Wang X, Feng W, Li H, Ruckenstein E (2001) Optimum toughening via a bicontinuous blending: toughening of PPO with SEBS and SEBS-g-maleic anhydride. Polymer (Guildf) 43:37–43. https://doi.org/10.1016/S0032-3861(01)00601-2

[43] Mozgawa W, Król M, Dyczek J, Deja J (2014) Investigation of the coal fly ashes using IR spectroscopy. Spectrochim Acta - Part A Mol Biomol Spectrosc 132:889–894. https://doi.org/10.1016/j.saa.2014.05.052

[44] Jeyageetha CJ, Kumar SP (2013) Study of SEM/EDXS and FTIR for fly ash to determine the chemical changes of ash in marine environment

[45] Smidt E, Böhm K, Schwanninger M The Application of FT-IR Spectroscopy in Waste Management

[46] Liu Y, Zeng F, Sun B et al (2019) Structural characterizations of aluminosilicates in two types of fly ash samples from Shanxi Province. North China Minerals 9:358. https://doi.org/10.3390/min9060358

[47] Hahn A, Vogel H, Andó S et al (2018) Using Fourier transform infrared spectroscopy to determine mineral phases in sediments. Sediment Geol 375:27–35. https://doi.org/10.1016/j.sedgeo.2018.03.010

[48] Deepthi MV, Sharma M, Sailaja RRN et al (2010) Mechanical and thermal characteristics of high density polyethylene-fly ash Cenospheres composites. Mater Des 31:2051–2060. https://doi.org/10.1016/j.matdes.2009.10.014

[49] Zhou J, Xia K, Liu X et al (2021) Utilization of cationic polymer-modified fly ash for dye wastewater treatment. Clean Technol Environ Policy 23:1273–1282. https://doi.org/10.1007/s10098-020-02019-2

[50] Fang J, Zhang L, Sutton D et al (2012) Needleless melt-electrospinning of polypropylene nanofibres. J Nanomater. https://doi.org/10.1155/2012/382639

[51] Jain D, Mishra M, Rani A (2012) Synthesis and characterization of novel aminopropylated fly ash catalyst and its beneficial application in base catalyzed Knoevenagel condensation reaction. Fuel Process Technol 95:119–126. https://doi.org/10.1016/j.fuproc.2011.12.005

[52] Dharmalingam U, Dhanasekaran M, Balasubramanian K, Kandasamy R (2015) Surface treated fly ash filled modified epoxy composites. Polimeros 25:540–546. https://doi.org/10.1590/0104-1428.2152

[53] Patil AG, Anandhan S (2015) Influence of planetary ball milling parameters on the mechano-chemical activation of fly ash. Powder Technol 281:151–158. https://doi.org/10.1016/j.powtec.2015.04.078

[54] Li JC, Zheng LF, Sha XH, Chen P (2020) Microstructural and mechanical characteristics of graphene oxide-fly ash cenosphere hybrid reinforced epoxy resin composites. J Appl Polym Sci 137:1–8. https://doi.org/10.1002/app.47173

[55] Ji Y, Yang X, Ji Z et al (2020) DFT-Calculated IR Spectrum Amide I, II, and III Band Contributions of N-Methylacetamide Fine Components. ACS Omega 5:8572–8578. https://doi.org/10.1021/acsomega.9b04421

[56] Gogoi R, Manik G (2021) Mechanical Properties of Wood Polymer Composites. Springer, Singapore, pp 113–136. https://doi.org/10.1007/978-981-16-1606-8_6

[57] Kulkarni SM, Kishore (2002) Effects of surface treatments and size of fly ash particles on the compressive properties of epoxy based particulate composites. J Mater Sci 37:4321–4326. https://doi.org/10.1023/A:1020648418233

[58] Doddipatla P, Agrawal S, Pilani B (2018) Effect of treatment of fly ash on mechanical properties of polypropylene. Key Eng Mater. https://doi.org/10.4028/www.scientific.net/KEM.759.20

[59] Yao W, Zhao Y, Wu K et al (2019) Effect of fly ash on the structure and properties of polyolefin elastomer/fly ash/

polypropylene composites. Mater Res Express 6:025308. https://doi.org/10.1088/2053-1591/aaed18

[60] Das A, Satapathy BK (2010) Structural, thermal, mechanical and dynamic mechanical properties of cenosphere filled polypropylene composites. https://doi.org/10.1016/j.matdes.2010.08.041

[61] Chand N, Vashishtha SR (2000) Development, structure and strength properties of PP/PMMA/FA blends

[62] Satapathy S, Kothapalli RVS (2018) Mechanical, dynamic mechanical and thermal properties of banana fiber/recycled high density polyethylene biocomposites filled with flyash cenospheres. J Polym Environ 26:200–213. https://doi.org/10.1007/s10924-017-0938-0

[63] Gogoi R, Kumar N, Mireja S et al (2019) Effect of hollow glass microspheres on the morphology, rheology and crystallinity of short bamboo fiber-reinforced hybrid polypropylene composite. JOM 71:548–558. https://doi.org/10.1007/s11837-018-3268-3

[64] Glass Transition Temperature (Tg) of Plastics - Definition & Values. https://omnexus.specialchem.com/polymer-propertie s/properties/glass-transition-temperature. Accessed 23 Jun 2021

[65] Sengupta S, Maity P, Ray D, Mukhopadhyay A (2013) Stearic acid as coupling agent in fly ash reinforced recycled polypropylene matrix composites: Structural, mechanical, and thermal characterizations. J Appl Polym Sci 130:1996–2004. https://doi.org/10.1002/app.39413

[66] Godara A, Raabe D, Bergmann I et al (2009) Influence of additives on the global mechanical behavior and the microscopic strain localization in wood reinforced polypropylene composites during tensile deformation investigated using digital image correlation. Compos Sci Technol 69:139–146. https://doi.org/10.1016/j.compscitech.2008.08.031

[67] Agarwal J, Mohanty S, Nayak SK (2020) Valorization of pineapple peel waste and sisal fiber: Study of cellulose nanocrystals on polypropylene nanocomposites. J Appl Polym Sci 137:49291. https://doi.org/10.1002/app.49291